

A multiscale framework for high-velocity impact process with combined material point method and molecular dynamics

Yan Liu · Han-Kui Wang · Xiong Zhang

Received: 23 December 2012 / Accepted: 1 February 2013
© Springer Science+Business Media Dordrecht 2013

Abstract The equation of state (EOS) plays an important role in high-velocity impact process since phase transformation, melting, and even vaporization may happen under such extreme loading conditions. It is desired to adopt an accurate EOS covering a large range of points in the phase space. This paper proposes a combined molecular dynamics and material point method approach to simulate the high-velocity impact process. The EOS data are first obtained from a series of molecular dynamics computations, and the parameters are fitted. Then the EOS parameters are adopted in the material point method simulation to model the impact process. Simulation results show that the fitted EOS can be very accurate compared to experimental results. The shape of the debris cloud obtained by our multiscale method agrees well with that of the experiments. An empirical equation is also proposed to predict the fraction of melting material in the high-velocity impact process.

Keywords High-velocity impact · Material point method · Molecular dynamics · Multiscale · Equation of state

1 Introduction

The projectile can impact the target with the velocity of the magnitude kilometres per second, which usually brings phase changes and even melting and vaporization (Zukas 1990). The typical velocity can even rise to more than 10 km/s in the space debris impact. It is very important to adopt appropriate equations of state (EOS) to describe material behaviors under high temperature and high pressure accurately in the high-velocity impact (HVI) process. Conventionally, the parameters of EOS mainly come from physical experiments, but unfortunately the experiments with high temperature and high pressure may be difficult and expensive to carry out. So only a limited part of points in the state space can be extracted from physical experiments, and other state points are predicted empirically based on some theoretical assumptions.

Molecular dynamics (MD) method (Rapaport 2004) provides a numerical way to simulate the physical process from the bottom atomic scale level. Some large-scale MD codes, for example, the LAMMPS code (Plimpton 1995), has been developed in recent years. The evolution of micro-structure can be analyzed by MD computations, and no macro-scale assumption is needed. The HVI problem being taken

Y. Liu · X. Zhang (✉)
School of Aerospace, Tsinghua University, Beijing
100084, People's Republic of China
e-mail: xzhang@tsinghua.edu.cn

Y. Liu
e-mail: yan-liu@tsinghua.edu.cn

H.-K. Wang
China Special Equipment Inspection and Research
Institute, Beijing 100013, People's Republic of China

as example, MD simulation can provide state points of the temperature and the pressure much higher than that in the experiments. MD, to some extent, can replace empirical EOS and material strength models. But the spatial and temporal scales of MD are still very limited, and it is not realistic to simulate the whole impact process with MD even when the size of the impactor is at microns and the physical time span is shorter than one microsecond. A macro-scale method must be included for real HVI simulation.

Even with appropriate EOS, numerical simulation of HVI problems may be unpractical due to severe mesh distortion or entanglement if the conventional mesh-based methods, such as Lagrangian finite element method (FEM), are used. The methods based on Eulerian description, such as the finite difference method or finite volume method, do not suffer from the mesh distortion, but the interfaces between different materials may diffuse in the computation. Mesh-free particle methods (Zhang and Liu 2004), which develop fast in recent years, show advantages over FEM in HVI simulation owing to no mesh dependence. Meshfree particles methods also show merits such as high accuracy, easy to deal with discontinuity and fragmentation, and easier pre-processing and post-processing.

Material point method (MPM) is one kind of meshfree particles methods. MPM was proposed by Sulsky et al. (1994, 1995) based on the idea of Particle-in-cell (PIC) method. MPM improved the accuracy of PIC by storing all the physical variables on the particles. MPM also employs a background mesh only to calculate gradients and solve equations of motion. So MPM possesses both the advantages of Lagrangian and Eulerian descriptions. As a meshfree particle method, MPM is much appropriate for simulating problems with large deformation, fragmentation, fracture and even phase changes. Recent studies have shown that MPM can be very efficient and effective in simulating impact problems. Chen et al. (2003) studies the dynamic failure of the brittle material under impact with MPM. Shen (2009) extends the method to rate-dependent material model and simulate the failure and fragmentation of glass. Zhang et al. (2009) applied MPM into the dynamic analysis of saturated porous subject to impact of solid bodies. Zhang et al. (2006) developed a material point finite element method (MPFEM), which utilized both the advantages of the MPM and the FEM. The object is initially discretized

by finite element mesh, then the finite elements can be converted to material points in large-deformation area. They successfully simulated hyper-velocity impact problems with MPFEM. Gong et al. (2012) proposed a MPM-based reconstruction technique to build true microstructure of aluminum foam from micro-CT images. They analyzed the shielding against space debris impacts with Whipple structure using the proposed method. Ma et al. (2009) compared MPM with another particle method, the smoothed particle hydrodynamics method (SPH), in detail. Their results show that MPM can be more efficient than SPH. Though the computational cost of every time step in MPM is heavier than that of FEM, MPM can even be more efficient in explicit analysis because large time step size can be used owing to no mesh distortion.

Some researchers combined MD and MPM to study localized problems with a multiscale method. Chen and his group (Shen and Chen 2005) focused on the delamination of tungsten film from the silicon substrate. They calculated the delamination problem at different scales. MD is used for the nano-scale while MPM is used in the macro-scale. They also proposed a smart boundary treatment to avoid the wave reflection on the boundaries (Shen and Chen 2006). Guo and Yang (2006) and Lu et al. (2006) developed handshaking technique for the concurrent MD-MPM multiscale method. Guo and Yang (2006) analyzed the generation and propagation of dislocation when the atom cluster impacts on the target. Lu et al. (2006) also shows that the results of the concurrent multiscale method agree well with the pure MD results. Liu et al. (2007) proposed an improved MD method, called the smoothed molecular dynamics (SMD), which employs the basic idea of MPM. A set of background mesh was introduced to MD calculation only to solve the equations of motion. The critical time step size of MD can be increased in orders, because the high-frequency oscillation was smoothed out. The overall accuracy of SMD solution is identical to that of MD since the motions of low frequency are described accurately (2007).

In this paper, MD and MPM are combined in another way to simulate the HVI problems from multiple scales. MD serves as a numerical EOS in MPM, and the macroscopic impact process is simulated with MPM. Sections 2 and 3 briefly investigate the theories of MD and MPM. Then the multiscale method is described in Sect. 4. The multiscale method is verified and validated in Sect. 6 by comparison with

experimental results and other numerical results. Section 7 concludes the whole paper.

2 Brief introduction to MD

MD method solves the following equations of motion

$$m_i \ddot{r}_i = F_i^{\text{int}}(r) + F_i^{\text{ext}}(r) \quad (1)$$

for each atom in the system. The collected behaviors of all the atoms will reflect macro properties of the simulated system. The subscript i is the atom index. m_i is the atom mass, the vector r_i denotes the atom position, and the vectors F_i^{int} and F_i^{ext} represent the internal forces and the external forces exerted on the atoms, respectively. The forces generally are functions of the positions of all the atoms, which are represented by the vector r in abbreviation. The overhead dot denotes the derivative with respect to time, for example \ddot{r}_i is the acceleration.

The internal forces between atoms, which are key factors to performances and reliabilities of MD results, can be calculated as the gradient of the potential $E_i^{\text{pot}}(r)$

$$F_i^{\text{int}} \equiv - \frac{\partial E_i^{\text{pot}}(r)}{\partial r_i} \quad (2)$$

Since the choice of the potential function has critical influences on MD results, many contributions have been made to propose appropriate potentials for different materials. Among many kinds of successful potentials for metals, the embedded atom method (EAM) potential (Daw and Baskes 1984; Johnson 1988), is a promising one. In EAM, the potential of atom i is composed by two parts,

$$E_i^{\text{pot}} = G_i(\rho_i) + \frac{1}{2} \sum_{j=1, j \neq i}^{n_{\text{atom}}} \phi_{ij}(r_{ij}), \quad (3)$$

where ϕ_{ij} is the pair potential between atoms i and j , $G_i(\rho_i)$ is the embedded potential which can be deemed as the energy caused by inserting the atom i into the electron environment. n_{atom} is the total number of atoms. The electron density ρ_i can be calculated by

$$\rho_i = \sum_{j=1, j \neq i}^{n_{\text{atom}}} f_{ij}(r_{ij}) \quad (4)$$

where $f_{ij}(r_{ij})$ is a prescribed function of the distance between two atoms.

Numerical schemes are required for time integration of Eq. (1). The velocity-Verlet scheme, one of the explicit schemes, is widely used. The velocity-Verlet scheme provides the procedure to update the positions and the velocities of the atoms from time level n to time level $n + 1$ explicitly

$$p_i^{n+1/2} = p_i^n + \frac{\Delta t}{2} F_i(r^n) \quad (5)$$

$$r_i^{n+1} = r_i^n + \Delta t p_i^{n+1/2} / m_i \quad (6)$$

$$p_i^{n+1} = p_i^{n+1/2} + \frac{\Delta t}{2} F_i(r^{n+1}) \quad (7)$$

where $p_i = m_i \dot{r}_i$ is the momentum of atom i , and the superscript n refers to variables at time level $n\Delta t$.

Some large-scale MD simulation codes for different kinds of materials have been released in recent years, of which the LAMMPS code (Plimpton 1995) is a typical one. LAMMPS is capable of dealing with many types of molecular/atomic systems with different kinds of potentials effectively. The LAMMPS code is adopted for the atomic-scale simulations to obtain EOS parameters in this paper.

3 MPM for HVI process

3.1 Discretization and evolution of physical variables

The MPM is a meshfree particle method. A set of discrete points, called the material points, are used to discretize the material domain. A set of uniform background mesh, which can be fixed in the space during the simulation or move in a designated way, is also employed to calculate the derivatives and serve as the scratch pad to solve the equations of motion. The discretization of the MPM is shown in Fig. 1. In every time step, the material points are assumed to be attached to and deform with the background grid, so that the physical variables on the particles can be approximated with those on background mesh nodes,

$$g_p = \sum_{l=1}^{n_e} N_{lp} g_l \quad (8)$$

where g is any field variable, and the subscript p denotes the particle number, the subscript l denotes the background node number. n_e is the total number of

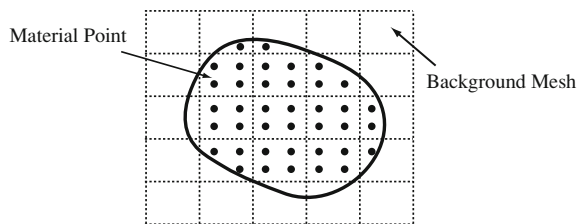


Fig. 1 Discretization in the MPM. A set of particles (denoted by circles) are used to discretize the domain (denoted by the area enclosed with solid line). Another set of background mesh (denoted by dotted lines) is used to calculate the derivatives and solve the equations of motion in every time step

nodes in the cell. $N_{Ip} = N_I(x_p)$ is the standard finite element shape function. For three-dimensional solid element, the shape function can be written as

$$N_{Ip} = \frac{1}{8}(1 + \xi_I \xi)(1 + \eta_I \eta)(1 + \zeta_I \zeta) \tag{9}$$

where ξ, η and ζ are the local coordinates of the particle, $(\xi_I, \eta_I, \zeta_I) = (\pm 1, \pm 1, \pm 1)$ are the respective local coordinates of the nodes.

The discretized equations of MPM can be derived from the weak form of the governing equations of updated Lagrangian description

$$\int_{\Omega} \delta v_{i,j} \sigma_{ij} d\Omega - \int_{\Omega} \delta v_i \rho b_i d\Omega - \int_{\Gamma_t} \delta v_i \bar{t}_i d\Gamma + \int_{\Omega} \delta v_i \rho \dot{v}_i d\Omega = 0 \tag{10}$$

by approximating the velocity v_i with Eq. (8)

$$v_{ip} = \sum_{I=1}^{n_e} N_{Ip} v_I \tag{11}$$

and approximating the density with the summation of discrete point masses by

$$\rho(x) = \sum_{p=1}^{n_p} \delta(x - x) m_p \tag{12}$$

where $\delta(x)$ is the Dirac delta function, and m_p is the mass of the particle p . In the above equations, v_i is the velocity vector, σ_{ij} is the stress tensor, ρ is the density, and b_i the body force per unit mass. δv_i is the virtual velocity. Ω is the solution domain, Γ_t is the traction boundary. \bar{t}_i is the prescribed traction on Γ_t . The subscript, “ j ” denotes the spatial derivative with

respect to the coordinate x_j . The final form of MPM discretized equations is

$$\dot{p}_{il} = f_{il}^{ext} - f_{il}^{int} \tag{13}$$

where

$$p_{il} = m_l v_{il} \tag{14}$$

is the momentum of the background node. It should be noted that the lumped mass $m_l = \sum_p m_p N_{Ip}$ has been adopted to ensure a fully explicit algorithm without solving a linear algebra system every time step. The external nodal force f_{il}^{ext} and the internal nodal force f_{il}^{int} are defined as follows,

$$f_{il}^{ext} = \sum_{p=1}^{n_p} N_{Ip} m_p b_{ip} + \int_{\Gamma_t} N_{Ip} \bar{t}_i d\Gamma \tag{15}$$

$$f_{il}^{int} = \sum_{p=1}^{n_p} N_{Ip,j} \sigma_{ijp} \frac{m_p}{\rho_p} \tag{16}$$

The discretized momentum equations, or the equations of motion, are set up on the nodes of the background mesh, though the physical variables are carried along with the material points. So the material points also serve as the quadrature points, similar to the Gauss integration in FEM. Detailed flowchart of the MPM and comparison with other meshfree particle methods can be found in literature (Ma et al. 2009).

3.2 Johnson–Cook material strength model

The Johnson–Cook plasticity material model has been widely used to describe material behaviors under high strain rate. The plastic flow stress σ_y are related with the effective plastic strain $\bar{\epsilon}^p$, the effective plastic strain rate $\dot{\bar{\epsilon}}$, and the temperature T in the following form

$$\sigma_y = (\sigma_0 + B \bar{\epsilon}^p) \left(1 + C \ln \frac{\dot{\bar{\epsilon}}}{\dot{\bar{\epsilon}}_0} \right) (1 - T^{*m}) \tag{17}$$

where $\dot{\bar{\epsilon}}_0$ is a reference strain rate to normalize $\dot{\bar{\epsilon}}$, and its value depends on the unit system. If the SI unit is used, $\dot{\bar{\epsilon}} = 1$; if the g–mm–ms unit system is used, the value will be 1,000. T^* is the normalized temperature defined by

$$T^* = \frac{T - T_r}{T_m - T_r} \tag{18}$$

where T_r and T_m are the room temperature and the melting temperature, respectively. σ_0 , B , C , n and m are material parameters that can be determined by experiments.

The failure of the material can be considered in Johnson–Cook model through accumulating the damage to one,

$$D = \sum \frac{\Delta \bar{\epsilon}^p}{\bar{\epsilon}^f} \tag{19}$$

where the fracture strain is determined by

$$\bar{\epsilon}^f = [D_1 + D_2 \exp D_3 \sigma^*][1 + D_4 \ln \dot{\epsilon}^*][1 + D_5 T^*] \tag{20}$$

where σ^* is the stress triaxiality p/σ_{eff} . p is the pressure, and σ_{eff} is the von-Mises effective stress. D_1 to D_5 are the material parameters.

3.3 GRAY equation of state

Some types of EOS, such as the Grüneisen equation of state, have been successfully used in the simulation of impact process, but very high impact velocities will pose more requirements on the equation of state. The ability to model complex phenomena of phase changes, melting, even vaporization may be required to analyze the HVI process accurately.

The GRAY equation of state, which was proposed in the technical report reference (Royce 1971), is appropriate for different phases of solid, liquid and gas of metals. The GRAY equation of state also has the ability to model transformations between phases. The phase diagram can be divided into a solid–liquid region and a liquid-vapor region. The boundary between the two regions are defined by $V = V_J$, any material beyond the specific volume V_J will be considered as vapor. The basic assumptions in GRAY model include

1. The melting entropy ΔS_m is independent of pressure, and it is approximately constant for a majority part of metals. $\Delta S_m = 1.16R$ for copper, where R is the gas constant.
2. The specific heat capacity, C_V , is the constant $3R$ for solid. While in the liquid regime, C_V decreases linearly with the temperature as the following,

$$C_v^{liq} = 3R - \alpha \frac{T}{T_m(V)} \tag{21}$$

3. The melting temperature T_m follows the modified Lindermann law

$$-\frac{d \ln T_m(V)}{d \ln V} = 2\gamma_m(V) - \frac{2}{3} \tag{22}$$

The scaling-law is used for material in solid–liquid region in GRAY EOS,

$$E_s(T, V) = E_0(V) + E_1(V)T + E_2(V)T^2 \tag{23}$$

$$P_s(T, V) = P_0(V) + P_1(V)T + P_2(V)T^2 \tag{24}$$

where E_s and P_s are the internal energy and the pressure, respectively. E_0 is the cold energy, P_0 is the cold pressure, T is the temperature, and V is the specific volume. E_1 , E_2 , P_1 and P_2 are coefficients relying on the specific volume, which are different in solid, melting, liquid, and hot liquid regimes. $\gamma_s(V) = \gamma_0 - ax$ and $\gamma_e = 2/3$ are the Grüneisen coefficients. The parameters to be determined are G , a and γ_0 . Detailed formulation of $E_i(V)$ and $P_i(V)$ can be found in Ref. (Royce 1971).

The vapor phase is described by Young–Alder equation

$$E = \frac{3}{2}RT - \frac{a_y}{V} \tag{25}$$

$$P = \frac{RT}{V} \frac{1 + z + z^2 - z^3}{(1 - z)^3} - \frac{a_y}{V^2} \tag{26}$$

where $z = V_b/V$. And a_y and V_b are material constants.

The formulations for the liquid and for the vapor are linked by smoothing functions $F_E(V)$ and $F_p(V)$,

$$E = \frac{3}{2}RT - \frac{a_y}{V} + F_E(V)(C_1 - C_3T^2) + (D_1 + D_2T + D_3T^2) \tag{27}$$

$$P = \frac{RT}{V} \frac{1 + z + z^2 - z^3}{(1 - z)^3} - \frac{a_y}{V^2} + F_p(V)(C_1 + C_2T + C_3T^2) \tag{28}$$

where

$$F_E(V) = \frac{V_b(\theta - z_J)^3}{2z_J^3} \left[\frac{2z - 2 + \theta}{(1 - z)^2} - \frac{2z_J - 2 + \theta}{(1 - z_J)^2} \right] \tag{29}$$

$$F_p(V) = \left(\frac{z \theta - z_J}{z_J \theta - z} \right)^3 \tag{30}$$

The coefficients C_1 , C_2 , C_3 , D_1 , D_2 , D_3 can be determined by the requirement that the equations of scaling

law and the Young–Alder equations should be seamlessly linked at $V = V_J$.

4 Multiscale framework

MD can simulate the behavior of the material from the atomic scale, but its ability is very limited. MPM can simulate the macroscopic scale phenomena, and an appropriate EOS is necessarily needed but difficult to measure. A natural way is to combine the advantages of the two methods. In this paper, MPM is selected as the macroscopic solver for HVI process, and MD is used to construct the EOS for MPM simulation.

A series of MD simulations are carried out to obtain the whole phase space. The system are initialized at a given temperature and a given volume. The system is relaxed to equilibrium to obtain the initial configuration. Then the temperature and the pressure of the system are changed step by step, and MD computations are run at each temperature and volume. The internal energy and other state variables are extracted from each simulation to obtain one point on the phase surface.

For current study of metal copper as example, one system consisting of 32,000 copper atoms is used throughout the simulation, and it should be pointed out that other kinds of metals can be simulated in the same procedure. All the atoms are set at ideal FCC sites with the lattice distance $a_0 = 0.3615$ nm. The periodic boundary conditions are applied at all the three directions so that a bulk material, from the macroscopic view, is simulated. At the beginning, the temperature of the system is set at room temperature, and then the system is relaxed with NVE ensemble for 30.0 ps. The temperature and the pressure of the system after relaxation are denoted by T_0 and P_0 respectively. Then we increase the pressure of system to $P_1 = P_0 + \Delta P$, where the pressure increment $\Delta P = 2.0$ GPa. The system after pressure increase is relaxed with NPT ensemble to obtain a system with the temperature T_0 and the specific volume V_1 , which is set as the starting point to obtain the state points with fixed specific volume V_1 but variable temperatures. The temperature of the system is increased to $T_1 = T_0 + \Delta T$, where the temperature increase $\Delta T = 100$ K. And one NVT simulation is executed at V_1 and T_1 , and one state point is recorded. After that another NVT simulation is executed at V_1 and $T_2 = T_1 + \Delta T$. Then the temperature is increased and more computations are executed

until the desired temperature T_{n_T} is obtained. Then the system pressure is increased again to and another loop for the temperature $T_1 - T_{n_T}$ are computed. The similar procedure is repeated with increasing the pressure until the designated pressure is reached. Therefore, one loop for the pressure and one loop for the temperature are employed to construct the surface. Totally $n_T \times n_P$ state points will be obtained. Figure 2 shows the procedure how to compute the phase points by MD simulation.

Then the data from MD simulation are used to construct the EOS. These data can be used to set up a table which supplies the state points by interpolation, or the data can be used to fit the parameters of specific EOS. The GRAY parameters are calculated in the current paper by the simulation points.

The fitted GRAY EOS is used in MPM to simulate the HVI problems. In the above framework, MD simulation serves as the numerical EOS, and MPM plays the role to simulate the whole impact process. Therefore a sequential multiscale framework is developed since the parameters for the macroscopic simulation is extracted from the microscopic simulations.

5 Projection technique for illustration of numerical results

The numerical results are usually compared with experimental results by configurations, such as the shape of the debris cloud, at different time points. Traditionally the numerical configurations are extracted from the results by clipping or viewing from specific angle. Though such configurations are natural to generate for comparison, they are actually different from the snapshots in the experiments. During the HVI experiment, X-rays are projecting to the path of the debris and make the film behind the specimen exposed. If more masses exist in some project direction, then more X-rays are scattered, and the projected image on the film will be darker. The schematic process to generate experimental images are shown in Fig. 3a.

Inspired by the imaging process in the experiments, a density projection technique is proposed to draw numerical ‘image’. All the material points are projected to a plane parallel to the projectile path of the debris. The gray scale of one pixel in the plane is obtained by converting the number of material points projected to the pixel. Large grey scale denotes more

Fig. 2 The procedure to compute state points with a series of MD simulations

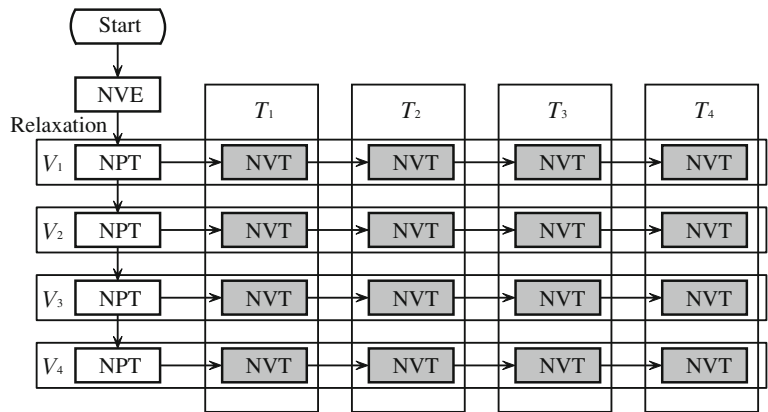
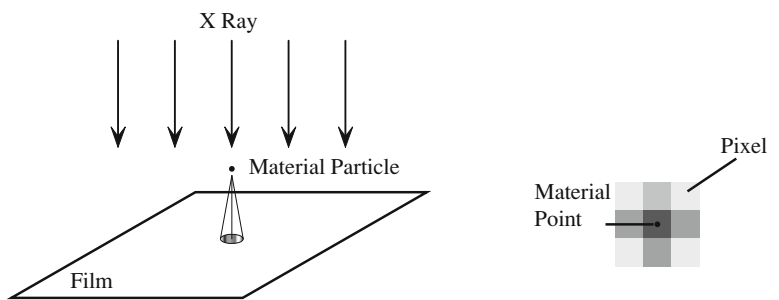


Fig. 3 Schematic illustration of (a) X-ray image and (b) the density projection technique



material points and is darker. The density of the debris cloud can be easily shown as a 2-D image by this method. Also, the projecting process is very similar to the exposure process of the film. So the numerical image and the experimental image can be comparable. The density projection method is shown in Fig. 3b.

6 Numerical examples

6.1 MD simulation results and fitted parameters

The copper system, which is described in Sect. 4, is calculated for $n_T \times n_P = 42 \times 51 = 2142$ points. The obtained surface in the phase space is shown in Fig. 4. A obvious belt of pressure jump can be observed, which corresponds to the melting region. The left lower region corresponds to the solid, while the right upper one is the liquid regime. The isothermal P–V curves, the isobaric V–T curves, and the adiabatic compressing curves can be extracted from the surface and compared to the experimental results.

The computed MD data can be used as a tabular to replace the EOS. Also, parameters in the EOS can be fitted by such data. We fitted the constants in GRAY EOS by running the following two optimization problems

$$\min f(C, S, \gamma_0, a) = \sum_{i=1}^{N_s} (P - P_i)^2 \quad (31)$$

$$S.t. : S > 0, C > 0, \gamma_0 > 0, \text{ and } a > 0 \quad (32)$$

and

$$\min f(T_m, g_e) = \sum_{i=1}^{N_s} (T - T_i)^2 \quad (33)$$

$$S.t. : T_m > 0, g_e > 0 \quad (34)$$

where γ_0, a, T_m, g_e are EOS parameters, and C and S are coefficients of the Hugoniot curve. They are categorized into two optimizations since the former four parameters influence much on pressure and the latter two are more related with temperature. The calculated parameters are compared with measured constants from experiments in Table 1. It is shown that V_0, C, S, γ_0 and a are close to the values reported in

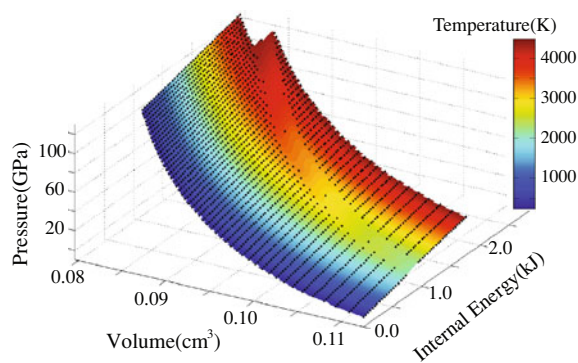


Fig. 4 The pressure-internal energy-specific volume surface. (The *color* denotes the temperature. The data are scaled by 1 g material). (Color figure online)

(Royce 1971). The differences of g_e and T_m are noticeable, which may be caused by the defects or inclusions, which exist in the true material but were not considered in the perfect lattice.

6.2 Validation of numerical EOS

Typical experiments to obtain EOS parameters can be categorized to dynamical experiments, such as a flyer impacting a thin plate, and quasi-static experiments such as indentation. Dynamical experiments can generate very high pressure but the loading time is very limited, so they are mainly used for Hugoniot curves. Quasi-static experiments can obtain high pressures in small spaces to construct the isothermal compression curve. The results from the dynamical and the quasi-static experiments will be compared with MD results.

Figure 5 compares the Hugoniot curve of the experimental results and the computational results. Solid line denotes MD results while the discrete triangles and circles denote the experimental results (Mitchell and Nellis 1981). It can be seen in the figure that the two results agree very well. MD results are only slightly lower than experimental results when the specific volume is less than $0.085 \text{ cm}^3/\text{g}$.

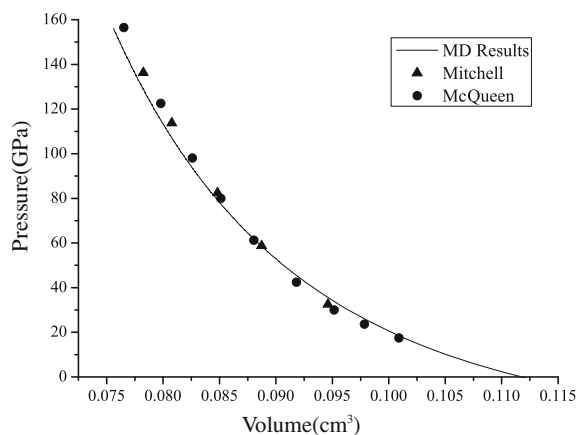


Fig. 5 Comparison of Hugoniot curves. *Triangles* and *circles* are experimental results (Mitchell and Nellis 1981). *Solid curve* denotes MD results

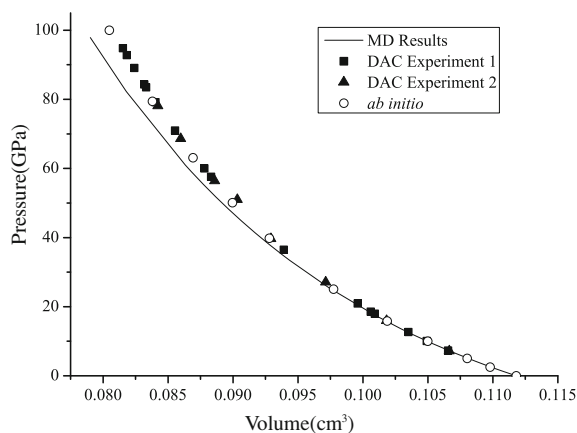


Fig. 6 Comparison of isothermal compression curves. *Solid squares* and *solid triangles* are experimental results (Pharr and Oliver 1992). *Solid curve* denotes MD results. *Hollow circles* are quantum mechanics results (Wang et al. 2000)

The isothermal pressure–volume curves are compared in Fig. 6. MD results (solid line) also agree well with experimental results (Pharr and Oliver 1992) (solid squares and solid triangles) and quantum mechanics results (Wang et al. 2000) (hollow circles). When the specific volume is less than $0.090 \text{ cm}^3/\text{g}$, MD results indicate small deviation from the experimental results, but the difference is less than 10 %.

Table 1 Fitted parameters of GRAY and comparison with experimental measurements (Royce 1971)

Parameters	V_0 (cm^3/g)	C ($\text{cm}/\mu\text{s}$)	S	γ_0	a	g_e ($\text{kJ}/\text{mole K}^2$)	T_m (K)
Experiment	0.1118	0.394	1.489	1.97	1.5	4.9×10^{-7}	1790
Numerical	0.1119	0.398	1.301	1.86	1.7	8.3×10^{-7}	2006

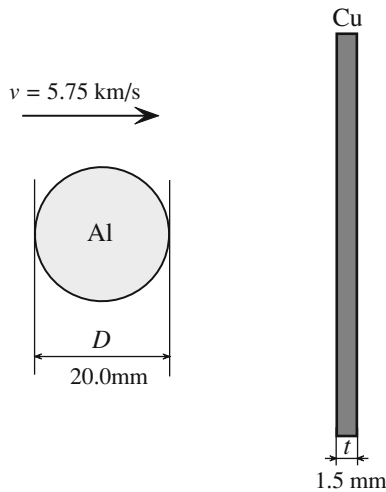


Fig. 7 Schematic illustration of the example of an aluminum sphere impacting on a copper plate

It can be concluded from the above results that MD computation can extract identical results with experiments when the compression is not very large. Large compression brings noticeable but acceptable difference, which may come from the influences of MD potential and the defects. The potential parameters are obtained from the situation that the atoms are not far away from the equilibrium position, which may lead to some deviations under high pressure and high temperature.

6.3 HVI examples

Two examples, including an aluminum projectile impacting on a copper target and a copper projectile impacting on an aluminum plate, are studied to further validate our method. In the first example, the projectile is a sphere of the diameter 20 mm and the impacting velocity is 5.75 km/s. The thickness of the target is

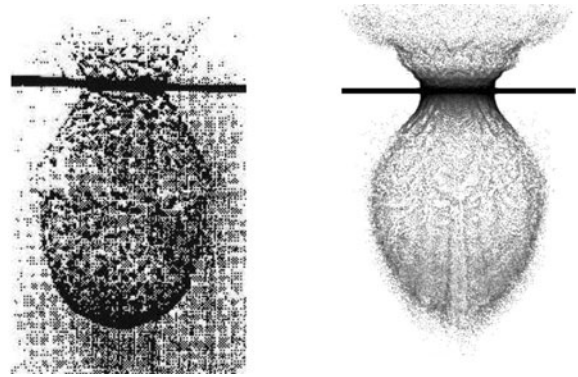


Fig. 8 Comparison of the experimental configuration (*left*) and the numerical configuration (*right*) of the debris cloud after an aluminum sphere impacting on a copper plate. The configurations are rotated clockwise for 90°

1.5 mm. The setup of the first example is illustrated in Fig. 7. The Johnson–Cook strength model is used for both copper and aluminum, and the material parameters are shown in Table 2. The EOS parameters for copper are extracted from MD simulation, and those for aluminum are from the references, which are listed in Table 3.

Figure 8 displays the debris cloud at 20 μs after the impact. The numerical configuration is very similar to the experimental snapshot. The numerical configuration is obtained by the density projection technique proposed in Sect. 5. Configurations and the phase distribution at $t = 1, 2$ and $5 \mu\text{s}$ are shown in Fig. 9. The center region of the debris cloud is melted or even becomes the hot liquid. But the melting region is limited and the border of debris cloud still remains solid though the materials are cracked and fragmented.

The second example is a copper cylindrical flyer impacting on an aluminum plate. As shown in Fig. 10, The diameter of the cylinder is 7.72 mm, and the height is 2.26 mm. The thickness of the target is

Table 2 Material parameters of Johnson–Cook plasticity model for the HVI examples

Parameters	E (GPa)	Poisson ratio	A (MPa)	B (MPa)	n	C	m
Aluminium	69	0.35	324	114	0.41	0.0	0.859
Copper	117	0.3	90	292	0.31	0.025	1.09

Table 3 Parameters of GRAY EOS for aluminum

Parameters	V_0 (cm ³ /g)	C (cm/μs)	S	γ_0	a	g_e (kJ/mole K ²)	T_m (K)
Aluminum	0.359	0.533	1.338	2.18	1.7	8.7×10^{-7}	1220

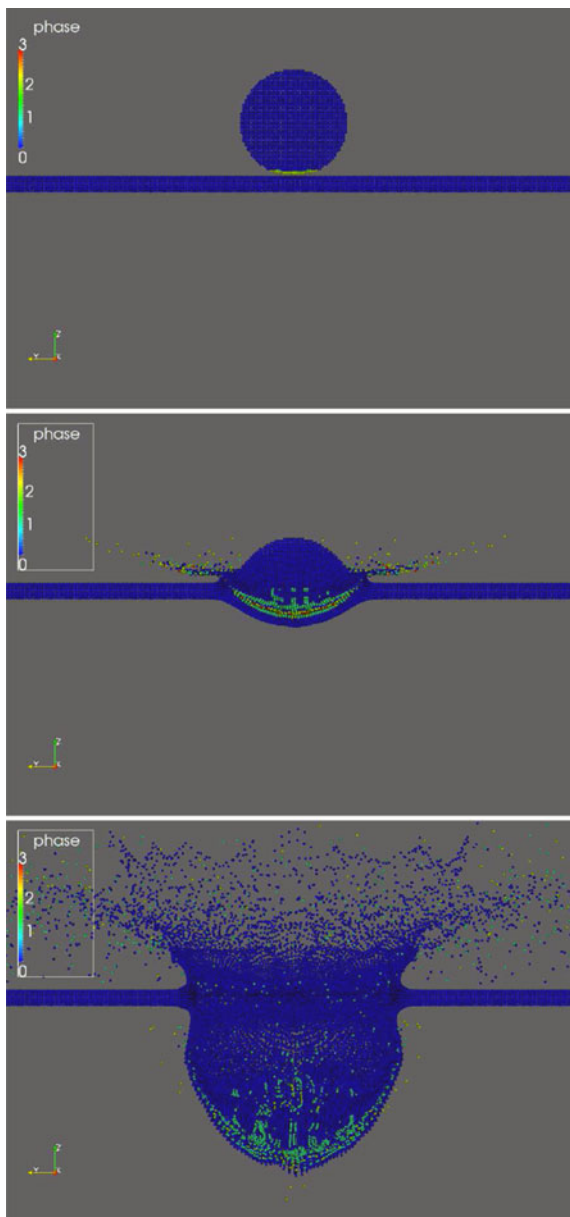


Fig. 9 Configurations and the phase distribution at $t = 1, 2$ and $5 \mu\text{s}$ (from the *top* to the *bottom*) of aluminum projectile impacting on copper target. The number 0, 1, 2, and 3 denote the solid regime, the melting regime, the liquid regime, and the hot liquid regime respectively

2.03 mm. The impact velocity is 6.23 km/s, which is a little larger than the previous example. As the impact process lasts very short time, it is difficult to change the films for different exposure, so one film is used throughout the experiment for multiple exposures. All the three experimental snapshots are shown in Fig. 11,

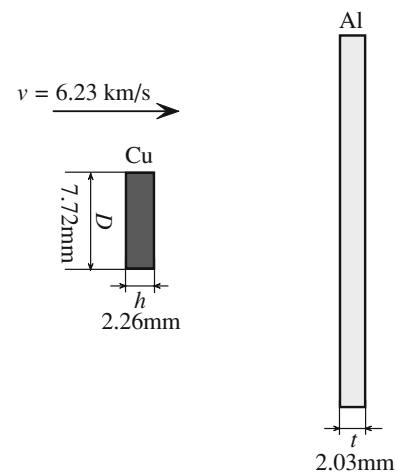


Fig. 10 Schematic illustration of the example of a copper cylinder impacting on an aluminum plate

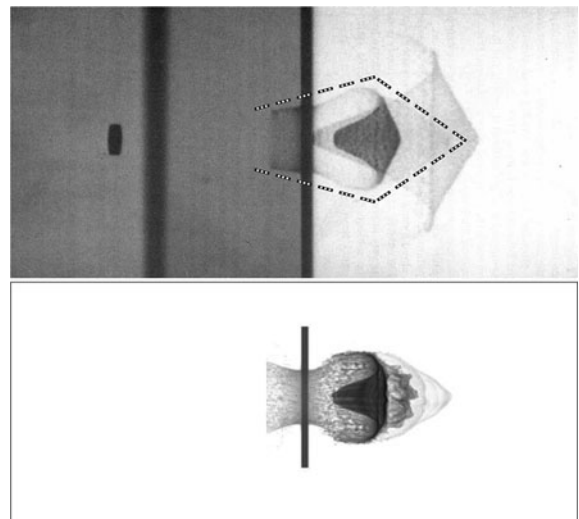


Fig. 11 Copper projectile impacting on aluminum target: the experimental configurations (*top*, enclosed by *dotted line*) and the numerical configuration (*bottom*)

of which the second snapshot, enclosed by the dotted line, is compared to the numerical configuration also shown in Fig. 11. The numerical results show the concentration of the material along the center line of the debris cloud. The phase and the configurations at other times are shown in Fig. 12, where the phase marked by the number “0” is the solid phase, “1” denotes the melting regime, “2” denotes the liquid phase, and “3” denotes the hot liquid.

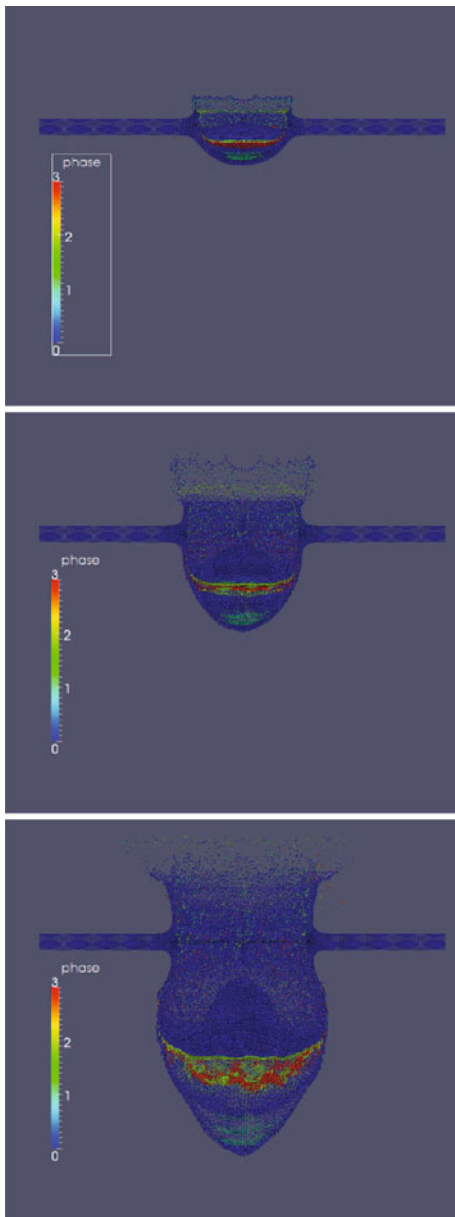


Fig. 12 Numerical results of copper projectile impacting on aluminum target at $t = 2, 3$ and $5 \mu s$ (from the top to the bottom). Different colors (numbered from zero to three) denote solid phase, melting regime, liquid phase and hot liquid phase, respectively. (Color figure online)

6.4 Empirical formulae of phase change and its validation

The fraction of the phase change of the material in the HVI process is studied. A copper sphere is projectiled onto a copper plate of the thickness $t = 2.5$ mm as

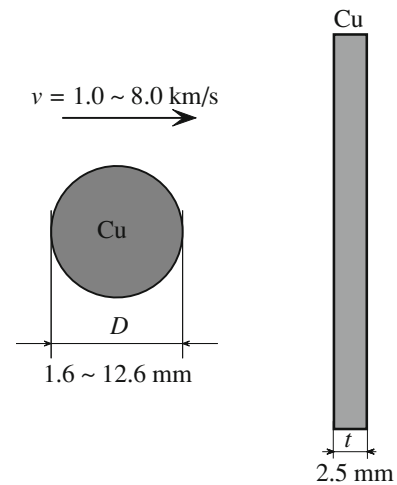


Fig. 13 The example for phase change investigation: a copper sphere impacting on a copper plate

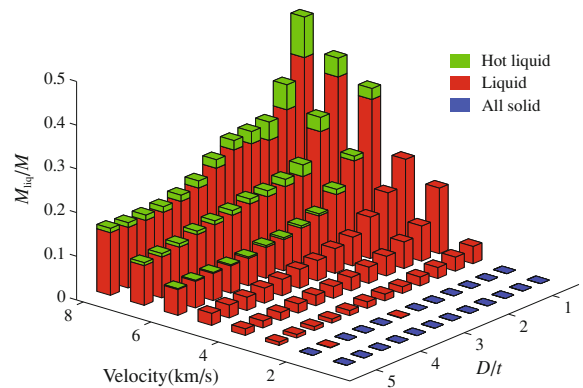


Fig. 14 The mass of the phase change material of the projectile, which is normalized by the total mass of the projectile. Red color denotes liquid metal, green color denotes hot liquid metal, and blue color denotes solid metal. (Color figure online)

shown in Fig. 13. The impact velocity and the size of the projectile are varied to investigate their effects on the phase change. The velocity varies from 1.0 to 8.0 km/s, and the diameter of the projectile are from 1.6 to 12.6 mm. The parameters of the material strength model and the EOS are the same as in the previous examples. The mass fraction of the phase change material of the projectile is shown in Fig. 14. Nearly no phase change happens when the impact velocity is less than 2 km/s, and hot liquid only appear when the velocity is higher than 6 km/s. The mass of the phase change material of the target, which is also scaled by the mass of the projectile, is shown in

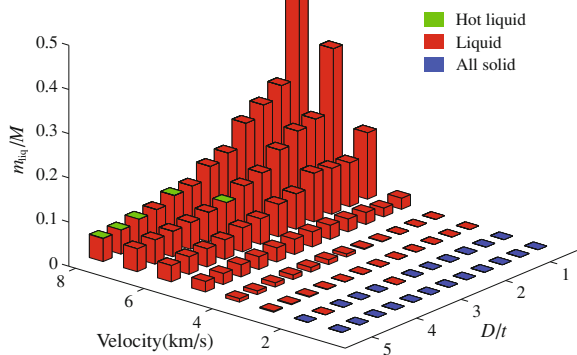


Fig. 15 The mass of the phase change material of the target plate, which is nondimensionalized by the total mass of the projectile. Red color denotes liquid metal, green color denotes hot liquid metal, and blue color denotes solid metal. (Color figure online)

Table 4 Parameters of the empirical formula

Parameters	α (km ⁻² s ²)	β (km ⁻¹ s)	γ
Value	6.480×10^{-3}	-7.515×10^{-3}	-0.6963

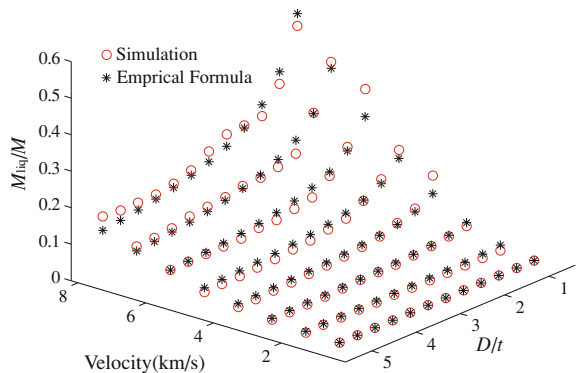


Fig. 16 Comparison of the empirical formula (marked by stars) and the simulated results (marked by circles)

Fig. 15. An interesting conclusion is that the fraction of the phase change of the target is much less than that of the projectile. Very little material changes to hot liquid only when the impact velocity is very high. Obvious phase changes are observed when the impact velocity is higher than 3 km/s.

The simulated data are fitted with the formula

$$\eta = (\alpha v^2 + \beta v) \left(\frac{D}{t}\right)^\gamma \tag{35}$$

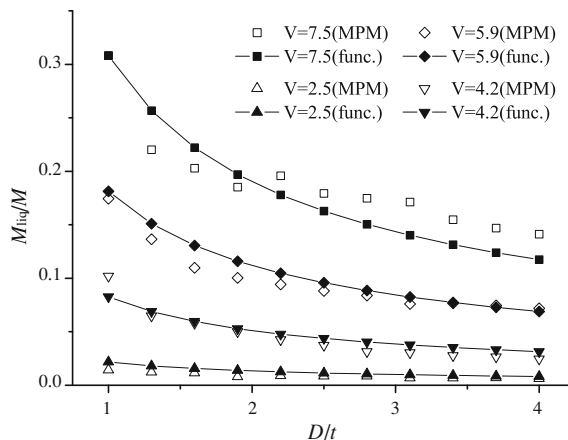


Fig. 17 Comparison of the empirical formula (marked by stars) and the simulated results (marked by circles) for the case the thickness is 5.0 mm

where η is the phase change fraction of the projectile. The fitted parameters α , β and γ are listed in Table 4.

Figure 16 compares the values calculated from the empirical formulae (35) and the computed results of the multiscale method. It can be seen that the formula can describe the phase change fraction at different impact velocities and diameters well. The empirical formula is further validated with the thickness of the plate $t = 5.0$ mm, which is shown in Fig. 17. The results at relative low velocities ($v = 2.5$ km/s and $v = 4.2$ km/s) can estimate the fraction of phase change well. The results of higher velocities ($v = 5.9$ km/s and $v = 7.5$ km/s) show some deviations, but the trend can be predicted.

7 Conclusion

As summary, we propose a computational framework combining MD and MPM to simulate the HVI processes. The EOS is constructed from a series of MD calculations, and the parameters of a specific EOS can be fitted from computed results. The numerical EOS is used in MPM computation for HVI simulation. The computational framework is validated in various ways by comparing Hugoniot curves and the isothermal compression curves from other references. The debris cloud of the HVI process is also compared, and the similar configurations to the experimental results can be obtained.

The phase changes in the HVI process are also investigated with the proposed multiscale method. An empirical formula is proposed to estimate the mass fraction of the phase change material of the projectile. The proposed formula is validated by the results of different thickness of the target.

The multiscale framework can be applied to the HVI process where the experimental results are difficult or expensive to carry out. MD simulations can provide state variables under high pressure and high temperature, and MPM has the ability to simulate problems of large deformation, crack, and fragmentation. The framework will be extended to other metal materials and the material with complex structures as the future development.

Acknowledgments Supported by National Natural Science Foundation of China (Grant No. 11102097) and National Basic Research Program of China (Grant No. 2010CB832701).

References

- Chen, Z., Feng, R., Xin, X. et al.: A computational model for impact failure with shear-induced dilatancy. *Int. J. Numer. Methods Eng.* **56**, 1979–1997 (2003)
- Daw, M.S., Baskes, M.I.: Embedded-atom method: derivation and application to impurities, surfaces, and other defects in metals. *Phys. Rev. B* **29**(12), 6443–6453 (1984)
- Gong, W.W., Liu, Y., Zhang, X., Ma, H.: Numerical investigation on dynamical response of aluminum foam subject to hypervelocity impact with material point method. *CMES Comput. Model. Eng. Sci.* **83**(5), 527–545 (2012)
- Guo, Z., Yang, W.: MPM/MD handshaking method for multiscale simulation and its application to high energy cluster impacts. *Int. J. Mech. Sci.* **48**(2), 145–159 (2006)
- Johnson, R.A.: Analytic nearest-neighbor model for FCC metals. *Phys. Rev. B* **37**(8), 3924–3931 (1988)
- Liu, Y., Zhang, X., Sze, K.Y., Wang, M.: Smoothed molecular dynamics for large step time integration. *CMES Comput. Model. Eng. Sci.* **20**(3), 177–192 (2007)
- Lu, H., Daphalapurkar, N.P., Wang, B., Roy, S., Komanduri, R.: Multiscale simulation from atomistic to continuum—coupling molecular dynamics (MD) with the material point method (MPM). *Philos. Mag.* **86**, 2971–2994 (2006)
- Ma, S., Zhang, X., Qiu, X.: Comparison study of MPM and SPH in modeling hypervelocity impact problems. *Int. J. Impact Eng.* **36**, 272–282 (2009)
- Mitchell, A.C., Nellis, W.J.: Shock compression of aluminum, copper, and tantalum. *J. Appl. Phys.* **52**(5), 3363–3374 (1981)
- Pharr, G.M., Oliver, W.C.: Measurement of thin-film mechanical-properties using nanoindentation. *MRS Bull.* **17**(7), 28–33 (1992)
- Plimpton, S.J.: Fast parallel algorithms for short-range molecular dynamics. *J. Comput. Phys.* **117**, 1–19 (1995)
- Rapaport, D.C.: *The Art of Molecular Dynamics Simulation*, 2nd edn. Cambridge University Press, Cambridge (2004)
- Royce, E.B.: A three-phase equation of state for metals. Tech. rep., Lawrence Livermore National Laboratory (1971)
- Shen, L., Chen, Z.: A multi-scale simulation of tungsten film delamination from silicon substrate. *Int. J. Solids. Struct.* **42**, 5036–5056 (2005)
- Shen, L., Chen, Z.: A silent boundary scheme with the material point method for dynamic analyses. *CMES Comput. Model. Eng. Sci.* **7**(3), 305–320 (2006)
- Shen, L.M.: A rate-dependent damage/decohesion model for simulating glass fragmentation under impact using the material point method. *CMES Comput. Model. Eng. Sci.* **49**, 23–5 (2009)
- Sulsky, D., Chen, Z., Schreyer, H.L.: A particle method for history-dependent materials. *Comput. Methods Appl. Mech. Eng.* **118**, 179–196 (1994)
- Sulsky, D., Zhou, S.J., Schreyer, H.L.: Application of a particle-in-cell method to solid mechanics. *Comput. Phys. Commun.* **87**, 236–252 (1995)
- Wang, Y., Chen, D.Q., Zhang, X.W.: Calculated equation of state of Al, Cu, Ta, Mo, and W to 1000 GPa. *Phys. Rev. Lett.* **84**(15), 3220–3223 (2000)
- Zhang, H.W., Wang, K.P., Chen, Z.: Material point method for dynamic analysis of saturated porous media under external contact/impact of solid bodies. *Comput. Methods Appl. Mech. Eng.* **198**, 1456–1472 (2009)
- Zhang, X., Liu, Y.: *Meshless Methods*. Tsinghua University Press, Beijing (2004)
- Zhang, X., Sze, K.Y., Ma, S.: An explicit material point finite element method for hyper velocity impact. *Int. J. Numer. Methods Eng.* **66**, 689–706 (2006)
- Zukas, J.A.: *High Velocity Impact Dynamics*. Wiley, New York (1990)